ELSEVIER

Journal of Hazardous Materials 62 (1998) 161–186

JOURNAL OF HAZARDOUS MATERIALS

An experimental study of the flow structure within a dense gas plume

Guwei Zhu, S. Pal Arya *, William H. Snyder [1]

Department of Marine, Earth and Atmospheric Sciences, North Carolina State University, Campus Box 8208, Raleigh, NC 27695, USA

Received 27 January 1997; revised 5 May 1998; accepted 6 May 1998

Abstract

A wind tunnel study was conducted to examine how a dense gas plume could affect the mean flow and turbulence structure of the boundary layer containing the plume. For this, a neutral atmospheric boundary layer developing over an aerodynamically rough surface was simulated in the US EPA's Meteorological Wind Tunnel. The dense gas plume was created by releasing CO_2 through a small circular source at ground level. A procedure was developed to make reasonably accurate mean velocity and turbulence measurements within the dense gas plumes by using hot-film anemometry in a range where the probe response was insensitive to the concentration of CO_2. Both the flow visualization and quantitative measurements of concentration and velocity fields indicated that, at low wind speeds, the dense gas plumes exhibited significant buoyancy effects on the flow structure. Within the dense plumes, mean velocity profiles were observed to have changed significantly in shape, with reduced speeds near the surface and increased velocities farther away from the surface. Consistent with these changes in mean velocity profiles, significant reductions in the roughness length and friction velocity were observed. Both the longitudinal and vertical turbulence intensities were also found to be greatly reduced within the dense plumes at low wind speeds. These changes in mean flow and turbulence structure were not only related to the dense-gas concentrations, but also to the local velocity gradients and the growth of the dense plumes with distance from the source. The local gradient Richardson number is found to be the most appropriate parameter for describing the changes in the mean flow and turbulence structure. Significant dense gas effects were observed when the Richardson number increased beyond its critical value (0.25) for the dynamic stability of a stratified flow. Our experimental results show

* Corresponding author. Fax: +1 919 515 7802

[1] Formerly with the National Oceanic and Atmospheric Administration, US Dept. of Commerce, on assignment to the US Environmental Protection Agency, Research Triangle Park, NC, USA.

PII: S0304-3894(98)00162-9

that, in an existing turbulent flow, turbulence is not completely suppressed even when the gradient Richardson number exceeds one.

Keywords: Concentration distributions; Dense gas dispersion; Flow visualization fluid modeling; Hazardous material; Modeling criteria; Plume dispersion; Turbulence intensities; Velocity profile

1. Introduction

Public concern over the risks posed by accidental releases of hazardous materials has increased markedly over the past few decades. The dioxin release in Seveso, Italy, in 1976, methyl isocyanate release in Bhopal, India, in 1984, and CO_2 release from Lake Nyos in Cameroon in 1986 are some of the better known examples of hazardous dense gas releases in concentrations high enough to kill thousands of people caught in their drifting plumes or clouds. Most of the dense gas dispersion modeling and experimental studies so far have focused on the growth of the dispersing cloud or plume as clean fluid is entrained in the same and the resulting concentration distributions [4,24]. It is generally assumed in models of dense gas dispersion that the background mean flow and turbulence are given and remain unaffected by the dense gas cloud or plume. Little work has been done on the possible effects of density stratification in dense gas plumes on mean velocity profile and turbulence which, in turn, have significant effects on the dense gas dispersion [17].

In a neutral surface layer, the mean velocity profile follows the well-known logarithmic law, irrespective of the surface roughness. Over an aerodynamically rough surface, the mean velocity distribution is given by [31,3]

$$U(z) = \frac{u_*}{k} \ln\left(\frac{z - d_o}{z_o}\right), \tag{1}$$

where $U(z)$ is the mean velocity at height z above the surface, u_* is the friction velocity, $k \simeq 0.40$ is the von Kàrmàn constant, z_o is the roughness length, and d_o is the zero-plane displacement height. The surface is considered aerodynamically rough if the roughness Reynolds number $\mathrm{Re}_* = u_* z_o/\nu \geq 2.5$ [31], although values as small as 0.5 have been found to be sufficient over roughness composed of sharp-edged obstacles (cf., Refs. [29,25]). The standard deviations of turbulent velocity fluctuations in the longitudinal and vertical directions within the fully developed (turbulent) neutral surface layer are approximately given as $\sigma_u \simeq 2.4u_*$ and $\sigma_w \simeq 1.25u_*$ [22].

However, when a large quantity of dense gas is released into a low-speed boundary-layer flow at or near the surface, previous studies have shown that a vertically thin but horizontally wide layer of dense-gas plume would be formed that may act like a 'vapor blanket'. The surface roughness elements, which make the surface aerodynamically rough, may be completely enveloped by this 'vapor blanket'. Due to negative buoyancy effects in the stably stratified dense-gas plume, the near-surface turbulence may be significantly suppressed, similar to the situation in a thermally stratified stable boundary

layer in which turbulence is found to be rapidly suppressed with increasing stability [18,1,2,36,14,20,26,16,21]. Since the friction velocity is also considerably reduced due to the stabilizing effect of the dense gas, the surface may become less rough or even aerodynamically smooth. The primary objective of this study was to investigate the possible stability effects of a dense gas plume on mean velocity profiles and turbulence intensities within the plume that grows in an otherwise neutral, rough-wall turbulent boundary layer. An experimental approach was used toward this end, utilizing the Meteorological Wind Tunnel of the US EPA's Fluid Modeling Facility in Research Triangle Park, NC. For the sake of simplicity, a neutral boundary layer over flat and uniformly rough terrain was simulated in the wind tunnel.

2. Modeling criteria and background

In an experimental dense gas plume study, similar to other fluid modeling studies, certain similarity requirements must be met so that the results from the small-scale experiment may be applied to the full-scale (prototype) situation in the atmosphere. These similarity requirements are usually obtained by dimensional analysis.

Although no specific atmospheric flow and dense gas release situation was modeled in this wind tunnel study, the consideration of similarity requirements between the model and the prototype was still considered to be important for planning of the experiments and also for possible comparisons between the results of this experiment with those from other model or field experimental studies. The possible independent variables that may be relevant to the particular situation of a dense gas plume in the neutral boundary layer over flat and uniformly rough terrain are:

U_r	Reference wind speed, taken here as the ambient wind speed just above the boundary layer
δ	Boundary layer thickness
h	Roughness element height
D_s	Diameter of the dense gas source
Q	Volume flow rate of dense gas
ρ, ρ_s	Densities of air and dense gas, respectively;
$\Delta\ \rho_o = \rho_s - \rho$	is the initial density difference at the source
υ, υ_s	Kinematic viscosities of air and dense gas, respectively
α	Molecular diffusivity of dense gas in air
g'_o	Reduced acceleration due to gravity in dense gas at the source; $g'_o = g\Delta\rho_o/\rho$

Of the above, the first three are boundary layer variables, D_s and Q are the source variables, the next five are molecular properties of air and the dense gas, and g'_o is the buoyancy variable. Here, we assume that the roughness parameter z_o and the friction velocity u_* are dependent variables whose values are determined by other boundary layer and roughness height parameters as well as by the buoyancy effects of the dense gas plume. Similarly, the dense gas plume height or thickness z_p is also considered a dependent variable, as it depends on both the boundary layer turbulence and effluent buoyancy effects.

The original eleven independent variables, involving three fundamental dimensions, yield at most eight independent dimensionless parameters which can be chosen as follows:

$\mathrm{Re}_\delta = U_r \delta/\upsilon$	The boundary layer Reynolds number
$\mathrm{Re}_s = W_s D_s/\upsilon_s$	The effluent Reynolds number
$\mathrm{Fr} = U_r/(g'_o D_s)^{1/2}$	The initial densimetric Froude number or bulk Richardson number $\mathrm{Ri}_B = 1/\mathrm{Fr}^2$
$Q_* = Q/U_r D_s^2$	Dimensionless effluent flow rate
$\mathrm{Sc} = \upsilon/\alpha$	The effluent Schmidt number
ρ_s/ρ or $\Delta\rho_o/\rho$	The effluent density ratio
δ/h	Dimensionless boundary layer height
D_s/h	Dimensionless source diameter

For an accurate and faithful simulation, all the dimensionless similarity parameters as well as boundary conditions are required to be matched between the model and the prototype [28]. It is, however, not possible to match all the parameters simultaneously at a significantly reduced scale. In fluid modeling studies of the type conducted here, the scale ratio typically ranges between 1/1000 and 1/100. Some relaxation of similarity requirements is always made on the basis of physical considerations.

Due to the reduced length scale in the model, the Reynolds number turns out to be the most mismatched parameter. Fortunately, a good justification for this mismatch has been provided by the Reynolds-number independence hypothesis which states that ''the turbulent flow structure is similar at all sufficiently high Reynolds numbers'' [32]. In this study, a more practical criterion based on the roughness Reynolds number, $\mathrm{Re}_* = u_* z_o/\upsilon \geq 2.5$, was used to ensure that the simulated turbulent boundary layer was Reynolds-number independent and therefore similar to that in a neutral atmosphere (except for the Coriolis turning of wind direction with height which, because of the small distances simulated, is believed to be unimportant [28]). Surface layer similarity theory only requires that Re_* be larger than some critical value of the order of 1, which may actually depend on the type and distribution of roughness elements on the surface [25,29], in order to ensure that the surface is aerodynamically rough and turbulence near the surface is not unduly influenced by fluid viscosity. This criterion, of course, ignores the stabilizing effect of the dense plume itself; in the presence of the dense gas, larger Reynolds numbers may be required.

The initial densimetric Froude number (Fr), or the bulk Richardson number (Ri_B), is perhaps the most important parameter to be duplicated for the simulation of dense plume dispersion. Matching of Fr between the model and the prototype with a large-scale reduction would require the flow speed in the model to be reduced by factors of 10 to 30. However, it may not be desirable nor practically feasible to operate environmental wind tunnels at very low ambient wind speeds (say, less than 0.5 m/s). The Reynolds-number criterion also precludes operating at very low wind speeds.

Provided that the scale ratios are matched (say, D_s/h), then matching of the dimensionless effluent flow rate is equivalent to the matching of the velocity ratio W_s/U_r in the model and the prototype. This can easily be done, but at very low source emission rates in the model, the effects of negative buoyancy of the dense gas plume may become insignificant. Other parameters, such as the Schmidt number, the effluent density ratio,

and the dimensionless source size can easily be matched by appropriate choices of source and dense gas. The matching of the ratio δ/h is likely to be unimportant if the dense gas plume is largely confined to the surface layer. With some relaxation of this requirement, a scale ratio of about 1:100 between the model and the prototype can be used, permitting simulations of wind speeds and source emission rates that are commonly encountered in the real world.

Whereas u_* is a dependent variable that will be affected by the presence of the dense gas plume, it is customary to characterize a dense gas release (continuous plume) by a source Richardson number

$$\mathrm{Ri}_\mathrm{o} = \frac{g'_\mathrm{o} Q}{D_\mathrm{s} u_*^3}.$$

Ri_o may be regarded as the ratio of the potential energy due to density excesses inside the dense cloud to the kinetic energy of the ambient turbulence. Plumes with small values of Ri_o are dominated by ambient turbulence and dense gas effects are insignificant. Dense gas effects gradually become important as Ri_o increases from about 1 to 100 with a 'critical' value of 50 [11]. We will use this parameter to characterize our releases.

Previous experimental studies of the possible effects of stratification in dense plumes on the mean flow and turbulence structure of the background boundary layer or channel flow are very few and far apart. Ellison and Turner [9] studied the mixing process of a dense layer of salt solution in a turbulent pipe flow. They observed significant distortion of the mean velocity profile with increasing stratification or Richardson number. The ratio of the Eddy diffusivities of salt and momentum was also found to be strongly dependent on Richardson number; $K_\mathrm{s}/K_\mathrm{m}$ decreased with increasing Ri. In a more recent study, Stretch [30] investigated the stratification effects of dense gas (CO_2) plumes on turbulence in a wind-tunnel boundary layer. His measurements showed that turbulence intensities within the dense plumes were significantly reduced due to stable stratification, while mean velocity profiles remained unaffected by the presence of the dense gas. The accuracy of the pulsed-wire probe used by Stretch [30] for measuring velocities within highly concentrated CO_2 plumes is, however, likely to be low and somewhat questionable. We found that pulsed-wire, hot-wire and hot-film probes are fairly sensitive to the presence of CO_2 in high concentrations and requires special calibration and operating procedures to obtain accurate results [38].

3. Experimental setup and instrumentation

3.1. Wind tunnel

The experiments were carried out in the US EPA's Meteorological Wind Tunnel [27], which has a test section 2.1 m high, 3.7 m wide, and 18.3 m long. The ceiling of the tunnel is adjusted to produce a zero-pressure-gradient boundary layer. The ambient wind speed in the test section can be varied from 0.3 to 8 m/s, but in the present study ambient wind speeds of 0.5, 0.75, 1.0 and 2.0 m/s were used. The simulated neutral

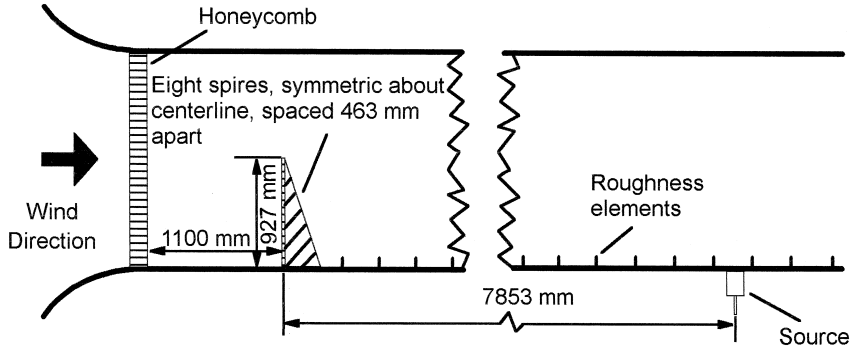

Fig. 1. Layout of wind tunnel.

atmospheric boundary layers were developed using the Irwin [13] system of eight equally spaced 927 mm high 'spires'. An aerodynamically rough surface was simulated using a uniform array of 25 mm high by 102 mm wide baffle plates which covered the entire test section floor downstream of the spires in a staggered pattern with 305 mm spacing between elements and rows. The side view of spires and baffle plates as roughness elements is shown in Fig. 1. This setup resulted in a 1 m deep boundary layer with a roughness length $z_o \simeq 1.2$ mm and a roughness Reynolds number $\mathrm{Re}_* \simeq 2.4$ at the lowest ambient wind speed of 0.5 m/s.

3.2. Dense gas source

Carbon dioxide (CO_2), with a molecular weight of 44 (1.52 times heavier than air), was chosen as the dense gas for this study because, compared with other heavy gases, it has smaller effects on the responses of hot-wire and hot-film anemometers [33]. Ethane (C_2H_6), mixed 3% by volume with CO_2, was used as a hydrocarbon tracer for concentration measurements.

The source gases were emitted at a specified rate (30 000 cc/min for CO_2 and 900 cc/min for ethane) through a 104 mm diameter, 200 mm deep cylinder filled with 3 mm gravel. The top of the gravel was flush with the tunnel floor. The source was positioned halfway between two rows of roughness elements on the tunnel centerline at a location near the center of the test section, as shown in Fig. 1. Downstream of the source and in its absence, the boundary layer could be considered in approximate equilibrium in the sense that the normalized mean velocity and turbulence intensity profiles did not change significantly with distance. As the effluent rate was fixed, the source Richardson number Ri_o was varied by changing the wind speed.

With the selected source flow rate and diameter, the average effluent velocity at the source was approximately 0.059 m/s, which is an order of magnitude smaller than the ambient wind speeds used in this study. The boundary layer flow should not be significantly affected by the effluent momentum [6]. Flow visualization showed that the selected source geometry and flow rate produced plumes with significant dense gas behavior at low ambient wind speeds (≤ 1.0 m/s).

3.3. Concentration measurements

Concentrations of hydrocarbon tracer gas and, by inference, of CO_2 were measured using a fast-response flame ionization detector (FID) made by Cambustion, (Model HFR 400). The basic design follows that of Fackrell [10] in that the burner assembly is removed from the normal chassis location and installed directly in the wind tunnel. In the current study, a sampling flow rate of 60 cc/min with a sampling tube of 0.25 mm inside diameter and 150 mm long was used. With this setup, the FID response had an upper frequency limit of 155 Hz. The response of the FID to C_2H_6/air and CO_2/C_2H_6/air mixtures was investigated in a series of tests in which source mixtures were diluted with air at constant rates in an exponential dilution chamber [35]. Significant deviations from the 'theoretical' exponential curve were found at high ethane concentrations (typically above 2000 ppm) in air. The situation in the presence of CO_2 was even worse. A correction scheme was developed in which correction factors were obtained from dilution tests [38]. The correction factor increased with increases in concentration of ethane in both the ethane–air and ethane–CO_2–air mixtures. The results of our tests clearly showed significant effects of CO_2 on the response of the FID and the necessity of using a correction scheme. In earlier experiments, Stretch [30] did not mention any such effects or a correction procedure.

The FID output was sampled at the rate of 150 Hz for a duration of 120 s. It was corrected for background concentration which typically increased from 5 ppm at the start to 10 ppm at the end of the day.

3.4. Velocity measurements

A variety of hot-wire, hot-film and pulsed-wire anemometers was used for mean velocity and turbulence measurements during this study. Details of their calibrations and response characteristics are given by Zhu [38]. A pulsed-wire anemometer was used to measure the mean flow pattern below the tops of the roughness elements, where low-speed reversing and recirculating flows exist. This was done only in the absence of the dense gas plume. The minimum speed that could be detected was about 0.12 m/s. Ordinary, hot-wire procedures were followed for characterizing the simulated atmospheric boundary layer in the absence of plumes.

For measurements within the dense gas plume, we tested a variety of hot-wire and hot-film anemometers as well as the pulsed-wire anemometer. All were found to be sensitive to the presence of CO_2; since the hot-wire and hot-film showed the most promise, the pulsed-wire anemometer was not given further consideration. The sensitivity of the other anemometers increased with increasing CO_2 concentration [23]. But, at a fixed CO_2 concentration, the sensitivity also varied with the operating overheat ratio, so that an optimum overheat ratio could be determined for each anemometer. In particular, for CO_2 concentrations of less than 25%, both the platinum hot-wire anemometer with its optimum overheat ratio of 1.70 and the hot-film anemometer with a lower overheat ratio of 1.60 were found to be suitable for measuring velocities over a range of 0.3 to 1.1 m/s with an accuracy better than 5%. With a slightly lower overheat ratio, the hot-film probe was found to be more stable than the hot-wire probe and therefore the former was

used for subsequent measurements in the dense gas plumes. We used an end-flow cross-film probe to measure both the longitudinal and vertical velocities, their variances and covariances. Prior to each day's measurements, the voltage output of the hot-film anemometer was calibrated against the wind speed measured by a pilot tube or calculated from the movement of smoke puffs in a uniform ambient flow. A best-fit fourth-degree polynomial was found to be more suitable for calibration than the commonly used King's law, especially in the low-speed range of interest to us. Further details of the calibrations and intercomparison of the different hot-wire, hot-film, and pulsed-wire anemometers in the various air–CO_2 mixtures are given by Zhu [38].

4. Results and discussion

4.1. The simulated boundary layer

The mean flow and turbulence structure of the simulated boundary layer was investigated before introducing any dense gases. For this, an end-flow x-wire probe was used to measure mean wind, longitudinal and vertical turbulence intensities and Reynolds stresses at various locations in the test section, at ambient wind speeds from 0.5 to 4 m/s. Figs. 2 and 3 show the normalized mean velocity and turbulence intensity profiles

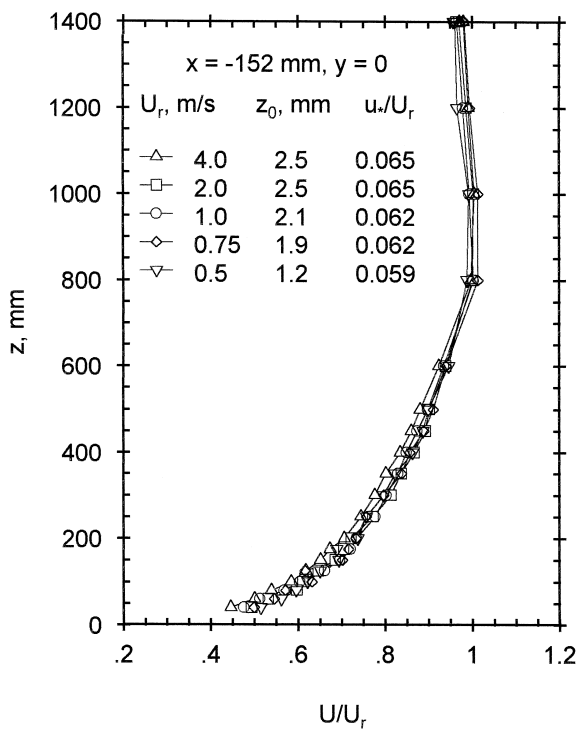

Fig. 2. Normalized mean velocity profiles at different ambient speeds.

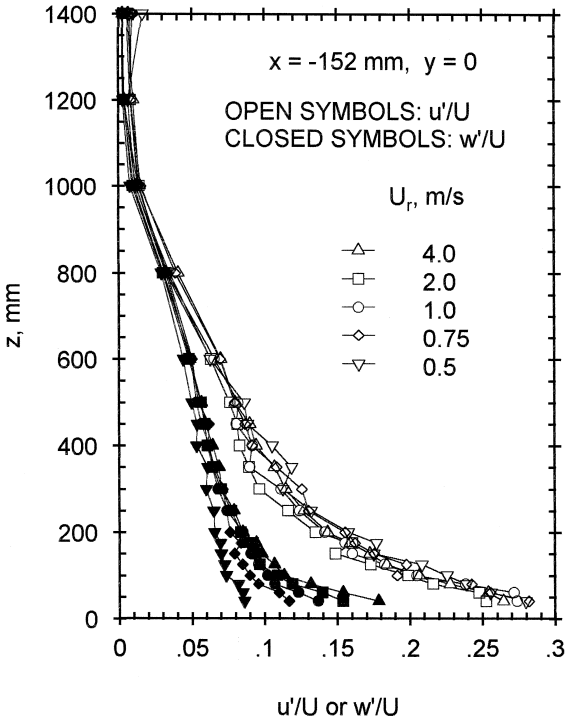

Fig. 3. Longitudinal and vertical turbulence intensity profiles at different ambient speeds.

slightly upwind of the source location. The measurements suggest that the vertical turbulence intensity and Reynolds stress decreased significantly near the surface as the ambient wind speed was reduced below 1 m/s. However, we believe that this is due to the poor yaw response of the hot-wire anemometer at low wind speeds (see, for example, Ref. [15]) and, thus, that the boundary–layer structure is essentially Reynolds-number independent over the whole velocity range (see also Ref. [29], for measurements over this same roughness geometry). The development of mean velocity, turbulence intensity and Reynolds stress profiles with downwind distance was observed to be so slow and gradual that the boundary layer may be regarded as essentially homogeneous in the longitudinal direction. The lateral homogeneity of the flow is also good, except close to the surface where the effects of individual roughness elements are clearly discernible. Significant influences of individual baffles could be seen up to two baffle heights or even higher at some locations [38].

The roughness length z_o in the simulated boundary layer was determined by best-fitting the measured mean velocity profiles between 50 mm (2 baffle heights) and 200 mm (about 20% of the boundary layer depth) to Eq. (1). For the widely spaced roughness elements used in this study, $d_o \simeq 0$. The friction velocity was determined from the smoothed profile of measured momentum flux ($\overline{u'w'}$), assuming that $u_*^2 \simeq -\overline{u'w'}$ at $z = 60$ mm. Then, using this u_* and with $d_o = 0$, Eq. (1) was best-fitted to

the mean velocity data in the height range 50 mm $\leq z \leq$ 200 mm to estimate z_o. As expected, the latter procedure yielded more consistent and stable estimates of z_o and u_*, which are given in Fig. 2. The apparent reduction in z_o and u_*/U_r with decreasing ambient wind speed is, again, believed to be due to the inadequate response of the hot-wire anemometer at the low wind speeds ($\leq$ 1 m/s).

4.2. Flow visualization of dense gas plumes

Before making any quantitative measurements in the dense gas plumes, flow visualization was conducted under conditions virtually identical to those under which the concentration and velocity measurements were made. Pure CO_2 and air with smoke were released through the source cylinder into the simulated boundary layer at the rates of 30 000 cc/min and 900 cc/min, respectively. Smoke was injected directly into the CO_2/air stream to visualize the emitted plume from the small circular source. Previous experience suggested that smoke added in this manner does not significantly alter the density of the source gas.

Two still and two video cameras were set up to take top and side views of the plume in the vicinity of the source. Pictures were taken nearly simultaneously with the two still cameras. The video cameras were used to record images of the plume continuously for each of the five ambient wind speeds (4, 2, 1, 0.75, and 0.5 m/s), including the transition period of change from one speed to another. Many still pictures and videos are included in the data collected for the study [37,38]. The pictures (not included here) show that significant dense gas phenomena were exhibited as the ambient wind speed was reduced to 1 m/s or lower; at and above 2 m/s the plume looked similar to that in the neutral plume (no dense gas) case. This corresponds with the critical $Ri_o \cong 50$ [11], as this plume with a 1 m/s freestream speed has $Ri_o = 109$, and at 2 m/s, $Ri_o = 14$. As the wind speed was decreased, the plume width increased laterally and the dense gas spread farther upwind from the source. For a fixed dense gas flow rate (source strength), the vertical depth of the plume decreased with decreasing wind speed, as the stabilization effect of the dense gas became more apparent. At the lowest wind speed of 0.5 m/s, some laminarization of the plume was observed below the tops of the roughness elements (baffle plates), especially near the source. Above the roughness element height, however, the plume appeared fully turbulent.

4.3. Concentration distributions and dispersion parameters

Longitudinal concentration profiles near the surface ($z = 5$ mm) in the various plumes are shown in Fig. 4. Fig. 5 displays the lateral concentration profiles at a distance of 1219 mm from the source. Similar measurements were also made at several other locations along the plume [38], but are not shown here. Both the longitudinal and lateral profiles at and below the roughness element height (25 mm) show significant effects of individual roughness elements on dense gas dispersion at low ambient wind speeds ($U_r \leq 1$ m/s or $Ri_o \geq 109$), not only near the source, but with diminishing effects also farther downstream.

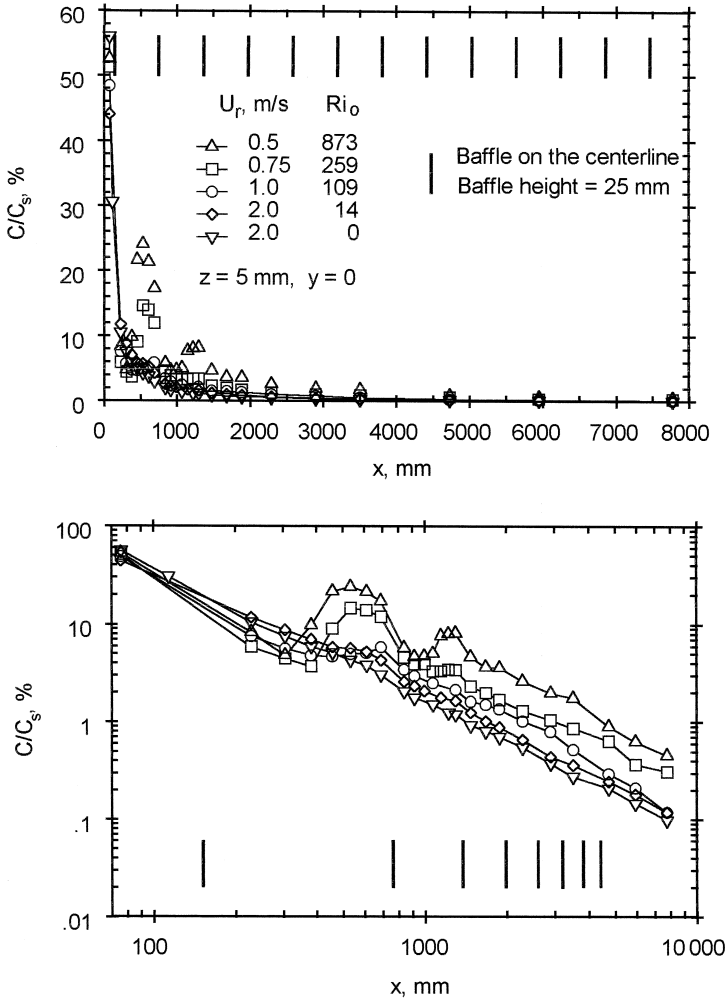

Fig. 4. Longitudinal ground level concentration profiles at $z = 5$ mm for different ambient wind speeds.

The effects of the baffle plates are more like those of obstacles rather than 'roughness' due to the fact that the plume heights are comparable to the plate height, particularly for the small distances ($x < 1000$ mm) and lower wind speeds.

Note that the roughness elements were arranged in a staggered or 'diamond' pattern and all lateral profiles were measured on a line halfway between two element rows. The concentrations immediately behind the plates were generally much smaller than those where no plate was in front of the sampling point. This is clearly shown in Fig. 5 where peaks in the lateral concentration profiles of the denser plumes line up perfectly with the baffle plates just downwind of the sampling line. Note that at this point the plume has already passed four rows of baffle plates, two with plates on the centerline and two with plates straddling it. This 'damming up' of heavy gas in front of the plates is also evident

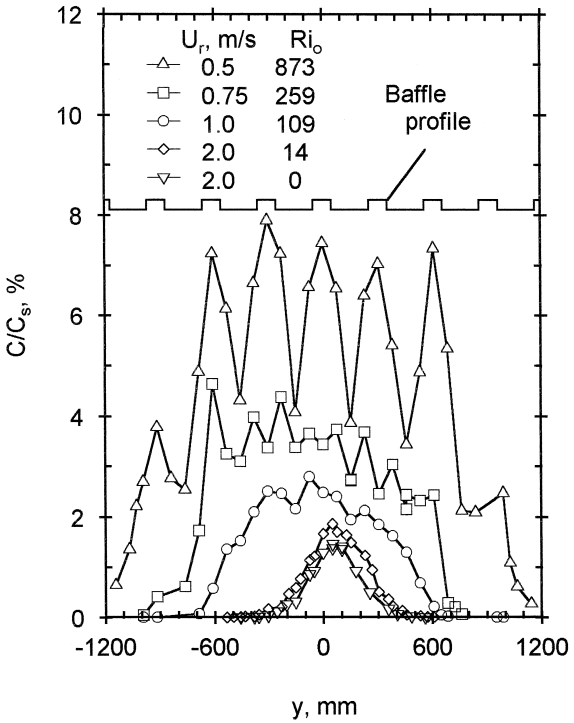

Fig. 5. Lateral concentration profiles at $x = 1219$ mm and $z = 5$ mm for different source Richardson numbers.

from the longitudinal profiles shown in Fig. 4. At wind speeds of 2 m/s and greater ($Ri_o \leq 14$), there was little difference between the dense gas and neutral plumes, as seen from the measured longitudinal and lateral concentration profiles. With decreasing wind speed, the ground-level concentrations along the plume centerline increased, especially after encountering the first row of roughness elements, and the plumes became much wider. In an earlier wind tunnel study of dense gas dispersion by Britter and Snyder [6], using the same wind tunnel, source geometry and CO_2 emission rate, but much smoother surface ($z_o = 0.13$ mm), smooth lateral concentration profiles were observed. The lateral distributions in both the present and the Britter and Snyder studies are very flat-topped with sharp tails and differ considerably from the Gaussian shape. It is clear that the buoyancy-induced lateral spreading, rather than turbulence, is responsible for the non-Gaussian distribution and much wider dense gas plumes as compared with neutral ones when, in our case, $Ri_o \geq 109$.

It is also noted that the ground-level concentration (glc) distributions downstream from the source (Fig. 4) differ from those shown by Snyder and Britter [6]. In addition to the irregularities due to the current baffle plates, our results show significant increases in glc's as Ri_o increases—as large as a factor of 5 when $Ri_o = 873$. For roughly the same value of Ri_o (109), Britter and Snyder showed glc's within 10% of the neutral plume values, whereas our current results show glc's nearly a factor of 2 larger than the neutral

plume values. This is evidently related to the shielding effect of the large elements and to the fact that the plume depth is not large compared with the baffle plate heights.

For a more quantitative analysis of dense plumes and their comparison with neutral plumes at the same ambient wind speeds, we characterize the four dense gas cases as D1, D2, D3, and D4, corresponding to ambient wind speeds of 0.5, 0.75, 1.0, and 2.0 m/s, respectively. The bulk dimensionless parameters of stability and source flow rate for the four dense gas cases are shown in Table 1. Here, we have also given values of the source Richardson number Ri_o and the dimensionless buoyancy parameter

$$Q_1 = g_o'^{2/5} Q^{1/5} U_{10}, \tag{2}$$

which was used by Britter and McQuaid [5] to reflect the overall stability of the plume. In the above definition, U_{10} denotes the wind speed at 10 m height (full scale), which is equivalent to that at 100 mm height in the wind tunnel, using a 1:100 scale. With the fixed dense gas emission rate and the constant density ratio or g_o' in the present study, Ri_o and Q_1, varied only due to changes in the wind speed. Thus, the range of Q_1 values essentially reflects a four-fold change in the ambient wind speed. Similarly, with the constant source diameter, the dimensionless dense gas emission rate Q_* varies in inverse proportion to the ambient wind speed. The bulk Richardson number has a much larger range because of its dependence on the inverse-square of the ambient velocity. The source Richardson number has an even larger range because of its dependence on the inverse cube of the friction velocity.

The most commonly used statistical measure of plume dispersion in the lateral direction is the standard deviation of the distribution (σ_y) around the plume centerline. For the dense gas plumes in our wind tunnel, the plume centerline near the surface was not always coincident with the tunnel centerline, but occasionally meandered to one side or the other due to uncontrollable disturbances and secondary flows in the wind tunnel at such ultra-low wind speeds. The variation of the plume dispersion parameter, σ_y, with distance from the source for the different plumes is shown in Fig. 6. Consistent with observations from the flow visualization, the plume width σ_y significantly increased with increasing source Richardson number Ri_o. Although σ_y generally increased with downwind distance from the source, as expected, leveling off and even a slight reduction of σ_y with increasing distance for the two most dense gas cases was observed. This may be due to the much flatter distribution of concentration in the lateral direction and larger effect of baffle plates on the same at shorter distances from the source, as compared to

Table 1
Values of bulk dimensionless parameters for the dense gas plume cases studied in the wind tunnel

Parameter	Dense gas plume cases			
	D1	D2	D3	D4
U_r (m/s)	0.50	0.75	1.0	2.0
Q_1	1.30	0.89	0.71	0.34
Ri_o	873	259	109	13.6
Ri_B	2.06	0.92	0.52	0.13
Q_*	0.092	0.062	0.046	0.023

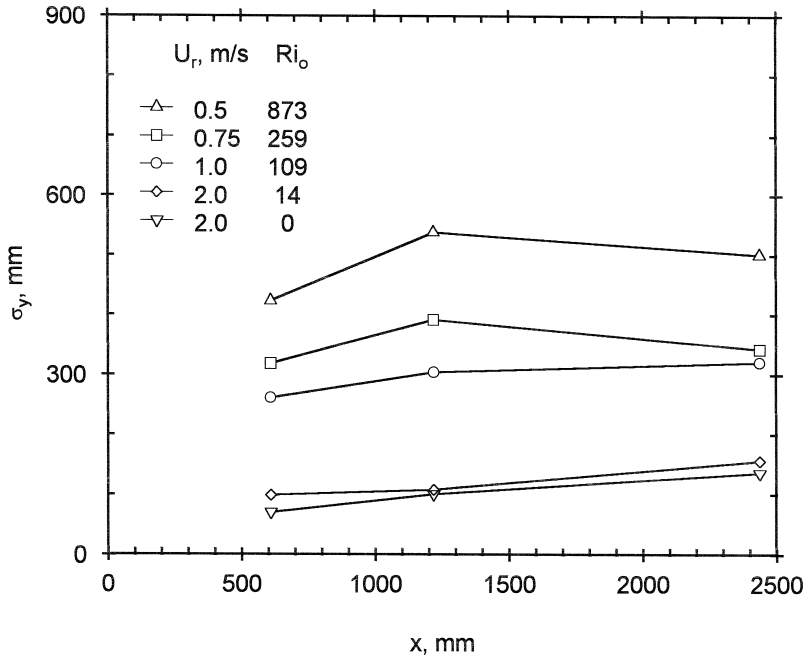

Fig. 6. Variation of the lateral dispersion parameter with distance from the source for different source Richardson numbers.

those at $x = 2438$ mm (see e.g. our earlier discussion of Fig. 5). The lateral concentration profiles at $x = 2438$ mm (not shown here) were more nearly Gaussian, with smaller undulations due to individual baffle plates [38]. No restrictive influence of side walls on the lateral plume spread was detected at that location.

Vertical concentration profiles were measured at four downwind locations on the centerline of the wind tunnel. A set of profiles measured at $x = 1219$ mm for the four different dense gas cases and one neutral case is shown in Fig. 7. More extensive concentration data are given elsewhere [37,38]. Many experimental and theoretical studies of vertical concentration distributions in neutral plumes from continuous ground-level sources have been conducted [19,33,12,7]. These have shown that the actual distributions are rarely Gaussian, but can be represented by the modified exponential form

$$C(x,z) = C(x,0)\exp\left[-B_\alpha(z/\bar{z})^\alpha\right], \tag{3}$$

in which $\bar{z}$ is the plume centroid height, defined as

$$\bar{z} = \int_0^\infty Cz\,\mathrm{d}z \Big/ \int_0^\infty C\,\mathrm{d}z \tag{4}$$

and B_α is a dimensionless constant which is uniquely related to the profile exponent or shape parameter α. In the stratified atmospheric boundary layer, α varies from 1 under

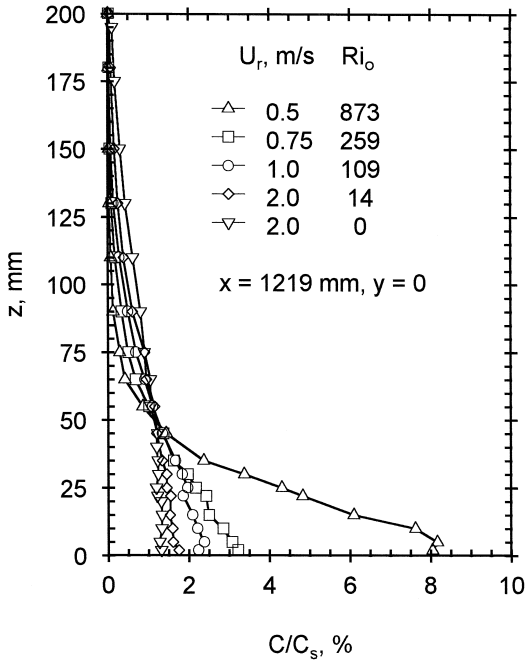

Fig. 7. Vertical concentration profiles at $x = 1219$ mm.

very unstable and convective conditions to more than 2 under very stable conditions. The commonly assumed Gaussian distribution, corresponding to $\alpha = 2$, is observed only under a rather narrow range of moderately stable conditions [19,20].

The limited observations of vertical profiles in dense gas plumes also confirm the non-Gaussian shape, with the profile shape parameter closer to one, implying an approximately exponential form [6]. The concentration distributions in dense gas plumes are substantially different from those in neutral plumes. The former are generally characterized by much higher ground-level concentrations and much smaller plume heights. A simple and commonly used measure of the plume height is z_p, the height where the concentration is reduced to 10% of the maximum (ground-level) concentration. Its variation with distance from the source and the plume buoyancy parameter is shown in Fig. 8. The strong influence of buoyancy on z_p is quite obvious. Another measure of mean plume height for surface releases is $\bar{z}$ defined by Eq. (4). The ratio $\bar{z}/z_p$ is 0.37 for a Gaussian distribution and 0.43 for an exponential one. $\bar{z}/z_p$ ranged from 0.36 to 0.49 for our plumes, with the larger values occurring with the denser plumes and closer to the source. Hence, our denser plumes have shapes tending toward exponential distributions, whereas the more neutral plume shapes tend toward Gaussian.

A comparison of the vertical concentration profiles measured during the present study with those from the Britter and Snyder [6] study, both using the same source geometry and flow rate but different surface roughnesses, indicates that the surface roughness also has significant influence on dense gas dispersion. In the present case, the plume depths

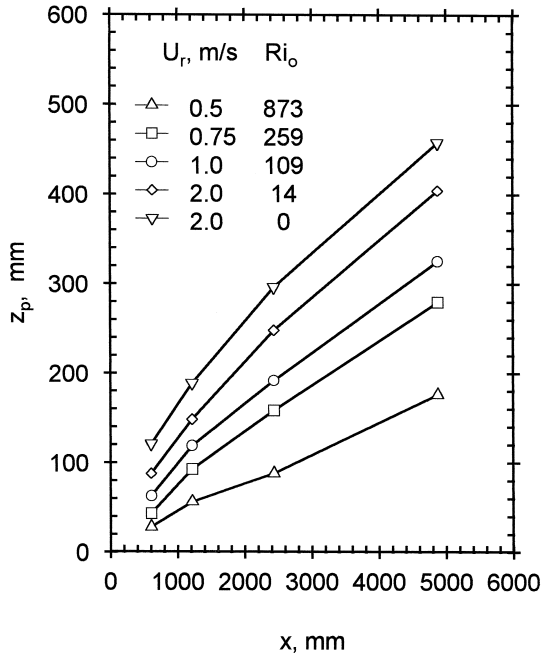

Fig. 8. Variation of plume height with distance downwind from the source.

were not large compared with the roughness element heights; indeed, the centroids of the denser plumes close to the source were less than the heights of the baffle plates, so that the plates appeared as individual obstacles to the plumes. In the Britter and Snyder study, the plumes were an order of magnitude deeper than the element heights, so that those plumes passed over a 'homogeneous' surface.

4.4. Mean velocity fields

As mentioned earlier, air flow near the surface is considerably influenced as it goes over and around individual roughness elements. Detailed information about the modified flow structure was obtained through the use of pulsed-wire as well as a hot-wire anemometer at a free stream wind speed of 4 m/s in the absence of any plume. The pulsed-wire measurements were focused on a typical region in and amongst the roughness elements; supplemental measurements were made above the elements using the hot-wire anemometer. By assuming that the mean flow pattern is symmetric about the vertical centerplane, the measured velocity vectors were used to deduce mean streamlines in the vertical (xz) center plane. By assuming the mean vertical velocities are zero very near the surface, mean streamlines in the horizontal (xy) plane were also deduced. The results are shown in Fig. 9. These streamline patterns clearly show large recirculating flow regions behind each roughness element in both the vertical and horizontal planes. The average length of the separated flow or cavity regions is about

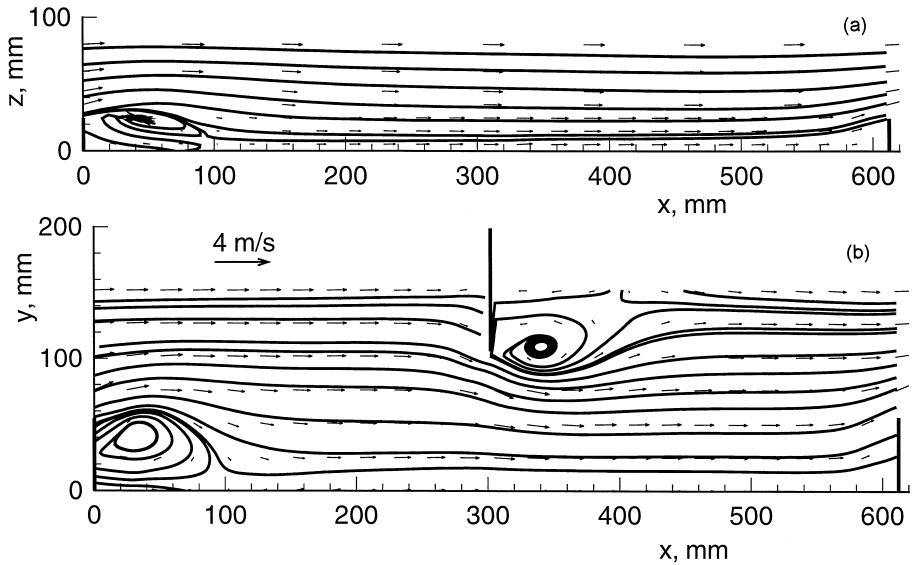

Fig. 9. Streamline patterns based on the pulsed-wire measurements in the roughness layer without any plume: (a) the *xz*-plane at $y = 0$; (b) the *xy*-plane at $z = 5$ mm.

four times the roughness element height. These recirculating flow regions were excluded from the subsequent hot-wire or hot-film measurements of mean flow and turbulence in the boundary layer and dense gas plumes.

Fig. 10 shows a comparison of mean velocity profiles in the lower part of the boundary layer with and without the dense gas plume. Note that at the lowest free

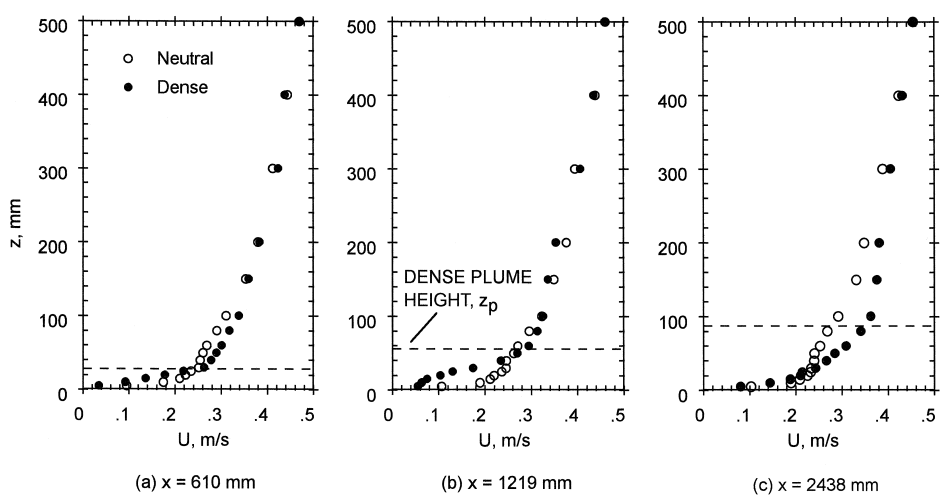

Fig. 10. Comparison of mean velocity profiles in the lower-half of the boundary layer with and without the dense gas plume for $U_r = 0.5$ ($Ri_o = 0$ and 873) at (a) $x = 610$ mm, (b) $x = 1219$ mm, and (c) $x = 2438$ mm.

stream velocity of 0.5 m/s ($Ri_o = 873$) mean velocity profiles were changed significantly by the presence of the dense gas. Mean velocities were reduced in the lower part of the plume, while they were increased in the upper part or above the plume height. The mean velocity gradient near the surface was also significantly reduced. These changes were not only related to CO_2 concentrations, but also to the growth of the plumes with distance. With increasing distance, the buoyancy-induced changes in velocity tend to propagate farther above the surface. As the ambient wind speed was increased to 0.75 and 1.0 m/s and, hence, Ri_o reduced, the influence of the dense gas on the mean velocity profiles also considerably diminished, although slight decelerations of flow near the surface and slight accelerations above could still be detected at $U_r = 1.0$ m/s ($Ri_o = 109$) [38]. Consistent with the reduced velocity gradient near the surface, the downward momentum flux $(-\overline{u'w'})^{1/2}$ was also substantially reduced with increasing Ri_o. From the estimated values of the friction velocity $(-\overline{u'w'})^{1/2}$ at $z = 60$ mm, we determined the ratio u_*/U_r for the various neutral and dense gas cases. The reduction in u_*/U_r is found to depend not only on Ri_o, but also on the distance from the source, as the buoyancy effects of the dense gas decrease with increasing distance. For example, at $x = 1219$ mm, u_*/U_r decreased from its nominal value of 0.060 for the neutral case to 0.044 for the most dense ($Ri_o = 873$) case. A similar (27%) reduction occurred at $x = 610$ mm, while a smaller (15%) reduction in u_*/U_r was observed at $x = 2438$ mm. There was some indication that the apparent surface roughness may also have been reduced by the stabilization effect of the dense gas plume. With significant deviations of the observed mean velocity profiles from the logarithmic law, however, it was not possible to determine z_o with a high degree of confidence.

4.5. Turbulence intensities

The stability or buoyancy effects of the dense gas plumes were most clearly seen in terms of reduced turbulence. A manifestation of this effect on downward momentum flux or u_* has already been discussed in Section 4.4. More important and relevant to plume dispersion are the turbulence intensities. The longitudinal and vertical turbulence intensities were measured with a cross hot-film anemometer at three ambient wind speeds and three positions downwind of the source, with and without the dense gas plume. Fig. 11 shows a comparison of the vertical turbulence intensities between the neutral ($Ri_o = 0$) and dense gas cases ($Ri_o = 873$) ($U_r = 0.5$ m/s in both cases). The growth of the dense gas plume is also depicted by a plot of the 10% plume height (z_p). Similar comparisons of longitudinal and vertical turbulence intensities for all the neutral and dense gas cases have been made by Zhu [38]. These show a systematic reduction in turbulence intensities with increasing Ri_o at any fixed position relative to the dense gas source. Fig. 11 shows that at the lowest ambient wind speed of 0.5 m/s, turbulence intensities in the dense gas plume were much reduced, even at large downwind distances. A part of this reduction is due to the modification of mean velocity profiles, as discussed in Section 4.4. However, direct suppression of turbulence by buoyancy or stability effects of the dense gas is largely responsible for the reduction in w'/U and u'/U, where w' and u' denote the standard deviations of vertical and longitudinal velocity fluctuations, respectively, and U is the local mean velocity.

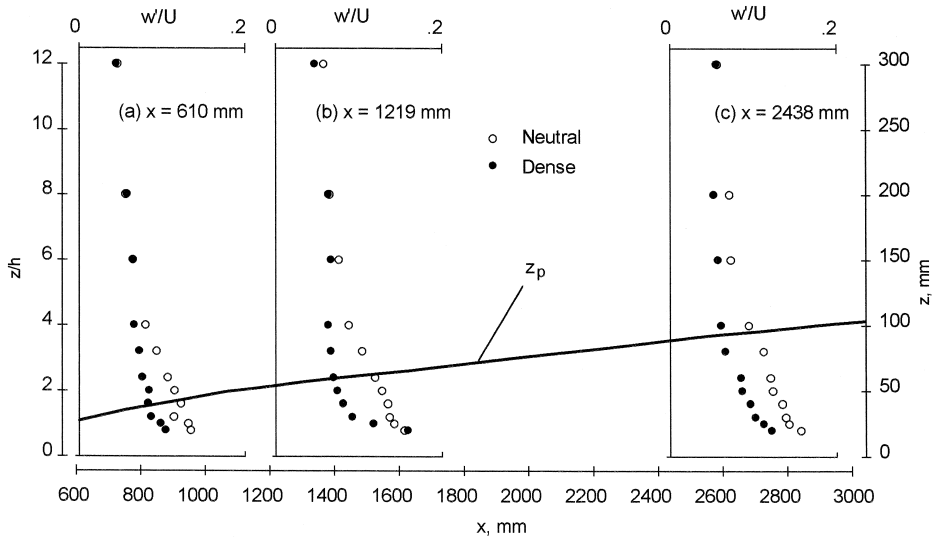

Fig. 11. Comparison of vertical turbulence intensities in the lower part of the boundary layer with and without the dense gas plume for $U_r = 0.5$ m/s ($Ri_o = 0$ and 873) at (a) $x = 620$ mm, (b) $x = 1219$ mm, and (c) $x = 2438$ mm.

The largest reductions in turbulence intensity occur at some distance from the source and away from the surface, as shown in the plots of percentage reductions in turbulence intensities in Figs. 12 and 13. At the lowest ambient wind speed ($Ri_o = 873$), the vertical

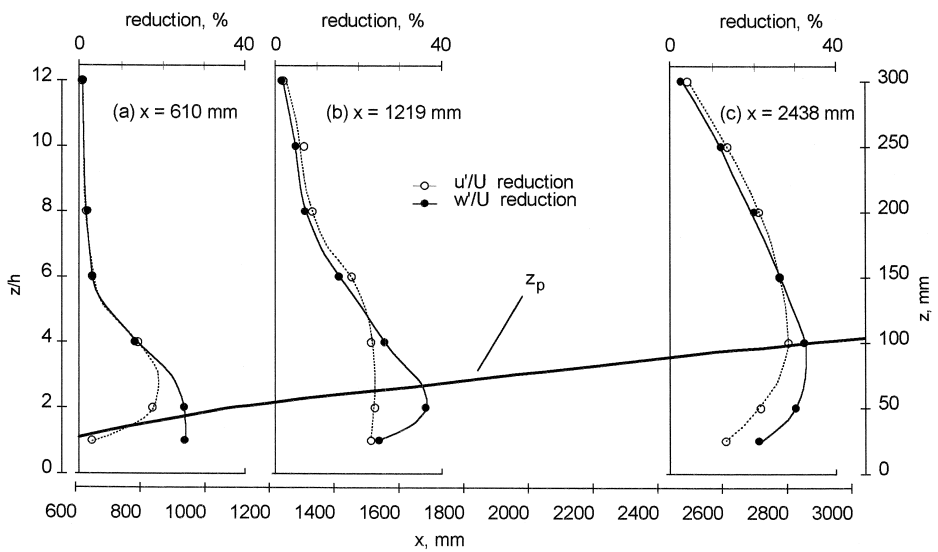

Fig. 12. Turbulence intensity reductions within the dense gas plume for $U_r = 0.5$ m/s ($Ri_o = 0$ and 873) at (a) $x = 610$ mm, (b) $x = 1219$ mm, and (c) $x = 2438$ mm.

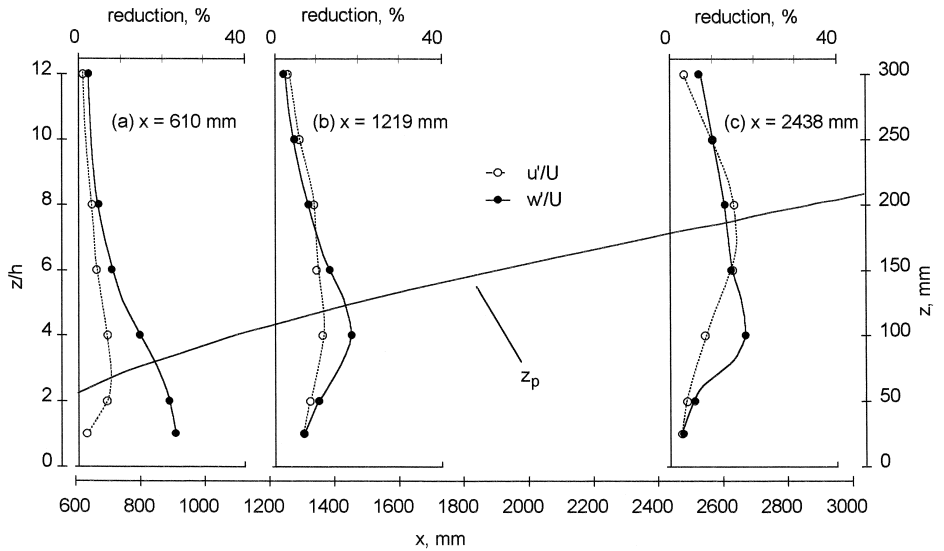

Fig. 13. Turbulence intensity reductions within the dense gas plume for $U_r = 1.0$ m/s ($Ri_o = 109$) at (a) $x = 610$ mm, (b) $x = 1219$ mm, and (c) $x = 2438$ mm.

turbulence intensity is reduced by more than 30% near the top of the dense gas plume. Even when $Ri_o = 109$ (minimum density effects), the maximum reduction is still close to 25%. Thus, the stability effects of the dense plumes are found to be much stronger on turbulence than on the mean flow, and these effects appear to persist for longer distances from the source and larger heights above the surface where the dense gas concentrations are much reduced. Significant reductions in turbulence intensities were observed up to distances twice as high as the 10% plume thickness. In the lower part of the dense plumes, both the longitudinal and vertical turbulence intensity reductions generally decreased with increasing distance from the source. They also decreased with increasing wind speed, whereas the height of the maximum reduction in turbulence intensity generally increased with ambient wind speed and also with downwind distance from the source. The reductions in turbulence intensities were not proportional or simply related to dense gas concentrations.

4.6. Local Richardson numbers

Having observed that the mean flow and turbulence structure of the lower part of a neutral boundary layer are significantly affected by stability or negative buoyancy of dense gas plumes, an attempt was made to relate the observed changes to a local stability parameter such as the local or gradient Richardson number

$$\mathrm{Ri} = -\frac{g}{\rho_o}\frac{\partial \rho}{\partial z} \Big/ \left(\frac{\partial U}{\partial z}\right)^2, \tag{5}$$

in which the density ρ is simply related to the dense gas concentration. For estimating Ri, both concentration and velocity profiles were smoothed appropriately.

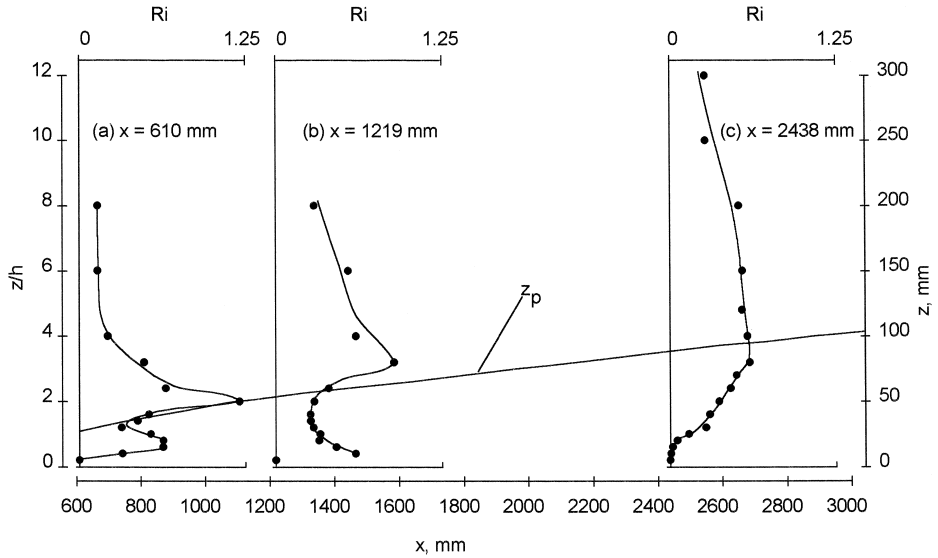

Fig. 14. Variation of gradient Richardson number with height in the dense gas plume for $U_r = 0.5$ m/s ($Ri_o = 873$) at (a) $x = 610$ mm, (b) $x = 1219$ mm, and (c) $x = 2438$ mm.

The vertical profiles of Ri at three downwind positions in the dense plume for the ambient wind speeds of 0.5 and 1.0 m/s ($Ri_o = 873$ and 109) are shown in Figs. 14 and 15. These profiles indicate that the local Richardson number attains its maximum value

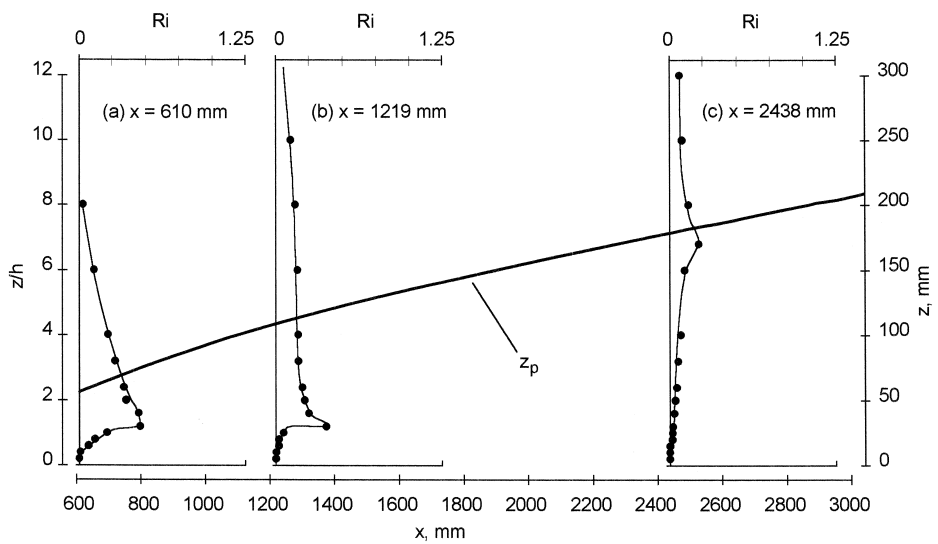

Fig. 15. Variation of gradient Richardson number with height for $U_r = 1.0$ m/s at (a) $x = 610$ mm, (b) $x = 1219$ mm, and (c) $x = 2438$ mm.

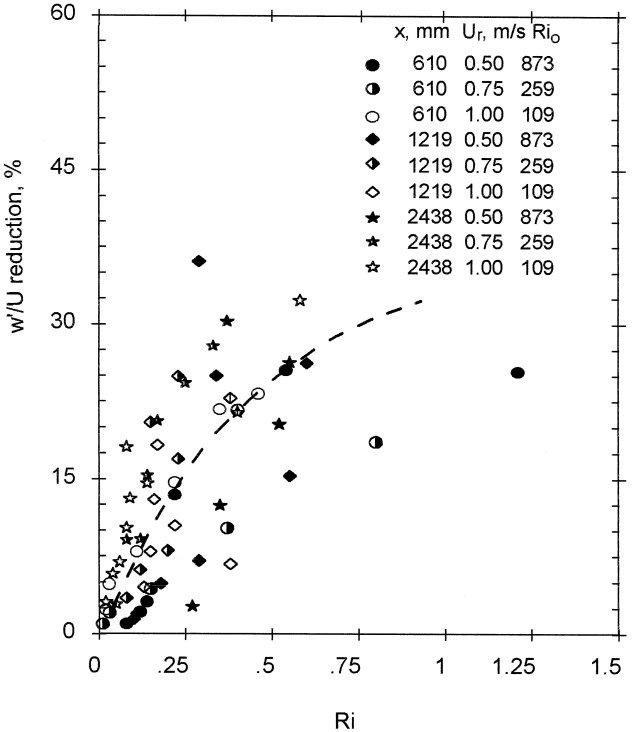

Fig. 16. Relationship between reductions in vertical turbulence intensities and local Richardson numbers for the three dense gas plumes.

in the same general location where turbulence intensities are most reduced. The largest Richardson numbers were observed at the lowest wind speed, as expected. Although the maximum value of Ri decreased with downwind distance from the source, the depth of the region of large Ri values (> 0.25) expanded. This may well explain why the observed reductions in turbulence intensities were quite significant even at large distances at low wind speeds. As the wind speed increased to 1.0 m/s, Ri values above 0.25 were mostly confined to short distances from the source. This is quite consistent with smaller reductions in turbulence intensities at large distances from the source.

The possible correlation between local Ri values and percentage reductions in vertical turbulence intensities is shown in Fig. 16. The large scatter is apparently not systematically related to ambient wind speed, distance from the source, or any dimensionless parameters. Despite this scatter, there appears to be a significant correlation between the percentage reduction in turbulence intensity and Ri. Large reductions in turbulence intensity generally occur where Ri is also large.

While the source Richardson number (Ri_o), Froude number, or the dimensionless source flow rate can only represent the overall effects of the dense gas plume on the mean flow and turbulence structure in the lower part of the boundary layer most affected by the plume, the local gradient Richardson number appears to be a more appropriate

parameter for more quantitative parameterizations of these effects in dense gas dispersion models. Further experimental studies of the effects of dense gas plumes on the flow structure, covering a much wider range of dimensionless buoyancy and source flow parameters than was possible in our study, may be necessary for developing more specific and reliable turbulence and dispersion parameterizations.

We have not addressed here the important question: Under what conditions might the turbulence be completely suppressed in a part of the dense gas plume? It is well known that turbulence in a stably stratified flow is destroyed by buoyancy when the flux Richardson number (Rf) exceeds its critical value $\mathrm{Rf}_c \leq 1$ (Richardson's criterion based on the turbulent kinetic energy equation). Other theoretical and empirical estimates of Rf_c lie between 0.15 and 0.5 [1]. In many experimental and observational studies, including the present one, flux Richardson number cannot be estimated because turbulent fluxes of momentum and scalar were not measured. The gradient Richardson number is easier to determine, but it may not always have a definite critical value above which turbulence disappears. Richardson's criterion for the maintenance of turbulence is strictly applicable to Rf rather than Ri. Since the relationship between the two

$$\mathrm{Rf} = \frac{K_s}{K_m}\mathrm{Ri} \tag{6}$$

involves the ratio of the eddy diffusivities of scalar and momentum, one can also express the same criterion in terms of Ri when the ratio K_s/K_m is close to one, as observed in the stable atmospheric surface layer. In most laboratory boundary layer and channel flows with stable stratification, however, the above ratio is found to decrease with increasing stability [9,34,2,21]. This implies that the critical value of Ri, if any, need not be less than one for the maintenance of turbulence. This is indeed confirmed by our results for the D1 and D2 cases ($\mathrm{Ri}_o = 873$ and 259) in which Ri exceeded one in a shallow elevated layer near the source ($x \leq 610$ mm) which remained fully turbulent. The criteria for the laminarization of a dense gas plume has been investigated in a separate study [8].

5. Conclusions

The primary objective of this experimental study was to examine the buoyancy effects of a dense gas plume on the mean flow and turbulence structure of the turbulent boundary layer in which the plume was embedded. The dense gas plume was generated by releasing CO_2 at a constant flow rate through a small, ground-level circular source. The US EPA's Meteorological Wind Tunnel was used to simulate the neutral atmospheric boundary layer over a moderately rough surface. The experimental results are presumably independent of Reynolds number, although low ambient wind speeds (0.5–1.0 m/s) required for simulating significant buoyancy effects in the dense gas plume did not permit the Reynolds number to become very large. In this study, we only required that the roughness Reynolds number, $\mathrm{Re}_* = u_* z_o/\nu$, be large enough to ensure an aerodynamically rough surface/flow for the simulated neutral boundary

layers. The same could not be confirmed, however, in the presence of the dense gas plume with strong buoyancy effects.

Both the qualitative flow visualization and quantitative velocity and concentration measurements showed that the dense gas plumes exhibited significant buoyancy effects when $Ri_o \geq 50$, in agreement with the criterion suggested by Hanna et al. [11]. Similarity considerations suggested several dimensionless buoyancy and source emission parameters which could be used as measures of overall buoyancy effects and also in formulating the appropriate similitude or modeling criteria. The local effects on mean flow and turbulence within the dense gas plume are found to vary considerably with height above the surface and with distance from the source. These could only be related to a local buoyancy parameter like the gradient Richardson number.

Mean concentration distributions in dense gas plumes were found to be quite different from those in neutral plumes, especially at low ambient wind speeds. Dense plumes may be characterized by larger lateral spread, smaller vertical spread, and higher ground-level concentrations. The buoyancy-induced horizontal spreading, rather than turbulence, is responsible for the non-Gaussian lateral distributions and much wider plumes as compared with the neutral plumes. The vertical distributions are also non-Gaussian and closer to an exponential shape. The negative buoyancy and reduced turbulence tend to make the dense gas plumes much thinner.

In the presence of the dense gas plume, the mean velocity profiles were changed significantly in shape near the surface at low wind speeds. Both the mean velocity gradient close to the surface and the friction velocity were reduced due to buoyancy or stability effects of the dense gas. Much larger effects (reductions) were found on longitudinal and vertical turbulence intensities. These changes in mean flow and turbulence were not only related to the local dense gas concentrations or vertical concentration gradients, but also to the vertical extent of dense gas plumes and ambient wind speeds (more appropriately, local velocity gradients). Therefore, the local gradient Richardson number (Ri) was used as an appropriate parameter for the local buoyancy effects on mean flow and turbulence. In particular, the percentage reductions in vertical turbulence intensities within the dense plumes appear to be well correlated with Ri. Significant dense gas effects were observed when and where Ri was greater than 0.25. However, turbulence was not completely suppressed even when Ri became greater than one. This implies that the ratio of the diffusivity of scalar (dense gas) to that of momentum is much less than one in dense gas plumes.

Acknowledgements

We are grateful for the cooperation and helpful assistance provided by Robert E. Lawson, Jr., G. Leonard Marsh and Michael S. Shipman at the Fluid Modeling Facility of the US Environmental Protection Agency in conducting these experiments. The third author acknowledges direct support from EPA, and the others through EPA Cooperative Agreement CR822057 with North Carolina State University. The contents of this paper do not necessarily reflect the views and policies of the funding agency, nor does the

mention of trade names or commercial products constitute endorsement or recommendation for use.

References

[1] S.P.S. Arya, The critical condition for the maintenance of turbulence in stratified flows, Q. J. Roy. Meteorol. Soc. 98 (1972) 264–273.
[2] S.P.S. Arya, Buoyancy effects in a horizontal flat-plate boundary layer, J. Fluid Mech. 68 (1975) 321–343.
[3] S.P. Arya, Introduction to Micrometeorology. Academic Press, San Diego, CA, 1988.
[4] R.E. Britter, R.F. Griffiths, Dense Gas Dispersion, Elsevier, Amsterdam, 1982, 247 pp.
[5] R.E. Britter, J. McQuaid, Workbook on the dispersion of dense gases, HSE Contract Res. Report No. 17/1988, Health and Safety Executive, Sheffield, UK, 1988.
[6] R.E. Britter, W.H. Snyder, Fluid modeling of dense gas dispersion over a ramp, J. Hazard. Mater. 18 (1988) 37–67.
[7] M.J. Brown, S.P. Arya, W.H. Snyder, Vertical dispersion from surface and elevated releases: an investigation of a non-Gaussian plume model, J. Appl. Meteorol. 32 (1993) 490–505.
[8] J. Ding, A wind tunnel study of flow laminarization in two-dimensional dense gas plumes. M.S. Thesis, Dept. of Marine, Earth and Atmospheric Sciences, North Carolina State University, Raleigh, NC, 1997.
[9] T.H. Ellison, J.S. Turner, Mixing of dense fluid in a turbulent pipe flow, J. Fluid Mech. 8 (1960) 514–544.
[10] J.E. Fackrell, A flame ionization detector for measuring fluctuating concentration, J. Phys. E: Sci. Instrum. 13 (1980) 888–893.
[11] S.R. Hanna, P.J. Drivas, J.J. Chang, Guidelines for Use of Vapor Cloud Dispersion Models, 2nd edn., Center for Chem. Process Safety, Amer. Inst. Chem. Engr., New York, 1996, 271 p.
[12] C.H. Huang, A theory of dispersion in turbulent shear flow, Atmos. Environ. 13 (1979) 453–463.
[13] H.P.A.H. Irwin, The design of spires for wind simulation, J. Wind Engr. Indus. Aerodyn. 7 (1981) 361–366.
[14] S. Komori, H. Ueda, F. Ogino, T. Mizushima, Turbulence structure in a stably stratified open channel flow, J. Fluid Mech. 130 (1983) 13–26.
[15] R.E. Lawson Jr., R.E. Britter, A note on the measurement of transverse velocity fluctuations with heated cylindrical sensors at small mean velocities, J. Phys. E: Sci. Instrum. 16 (1983) 563–567.
[16] D.H. Lenschow, H.S. Li, C.J. Zhu, B.B. Stankov, The stably stratified boundary layer flow over the Great Plains: I. Mean and turbulence structure, Boundary-Layer Meteorol. 42 (1988) 95–121.
[17] R.N. Meroney, Guidelines for fluid modeling of dense gas cloud dispersion, J. Hazard. Mater. 17 (1987) 23–46.
[18] A.S. Monin, A.M. Yaglom, Statistical Fluid Mechanics: Mechanics of Turbulence, Vol. 1, MIT Press, Cambridge, MA, 1971.
[19] F.T.M. Nieuwstadt, A.P. van Ulden, A numerical study of passive contaminants from a continuous source in the atmospheric surface layer, Atmos. Environ. 12 (1978) 2119–2124.
[20] Y. Ogawa, P.G. Diosey, K. Uehara, H. Ueda, Wind tunnel observation of flow and diffusion under stable stratification, Atmos. Environ. 19 (1985) 65–74.
[21] Y. Ohya, D.E. Neff, R.N. Meroney, Turbulence structure in a stratified boundary layer under stable conditions, Bound.-Layer Meteorol. 83 (1997) 139–161.
[22] H.A. Panofsky, J.A. Dutton, Atmospheric Turbulence, Wiley, New York, 1984.
[23] W.M. Pitts, B.J. McCaffrey, Response behavior of hot wires and films to flows of different gases, J. Fluid Mech. 169 (1986) 465–512.
[24] J.S. Puttock, Stably Stratified Flow and Dense Gas Dispersion, Oxford Science Pub., Oxford UK, 1988.
[25] M. Schatzmann, W.H. Snyder, R.E. Lawson, Experiments with heavy gas jets in laminar and turbulent crosswinds, Atmos. Environ. 27A (1993) 1105–1116.

[26] A.S. Smedman, Observations of a multi-level turbulence structure in a very stable atmospheric boundary layer, Bound.-Layer Meteorol. 44 (1988) 231–253.
[27] W.H. Snyder, The EPA Meteorological Wind Tunnel: Its design, construction and operating characteristics. Report No. EPA-600/4-79-051, US Environmental Protection Agency, Research Triangle Park, NC, 1979.
[28] W.H. Snyder, Guideline for fluid modeling of atmospheric diffusion, Report No. EPA-600/8-81-009, US Environmental Protection Agency, Research Triangle Park, NC, 1981.
[29] W.H. Snyder, I.P. Castro, Surface-Reynolds-Number Effects in Rough-Wall Boundary Layers, 1998, in preparation.
[30] D.D. Stretch, The dispersion of slightly dense contaminants in a turbulent boundary layer, PhD Dissertation, Univ. of Cambridge, Cambridge, UK, 1986.
[31] O.G. Sutton, Micrometeorology, McGraw-Hill, New York, 1953.
[32] A.A. Townsend, The Structure of Turbulent Shear Flow, Cambridge Univ. Press, Cambridge, UK, 1956.
[33] A.P. van Ulden, Simple estimates for vertical diffusion from sources near the ground, Atmos. Environ. 12 (1978) 2125–2129.
[34] C.A.G. Webster, An experimental study of turbulence in a density-stratified shear flow, J. Fluid Mech. 19 (1964) 221–245.
[35] H.P. Williams, J.D. Winefordner, Construction and operation of a single exponential dilution flask for calibration of gas chromatographic detectors, J. Gas. Chrom. (1966) 271–272.
[36] S. Yamamoto, O. Yokoyama, M. Gamo, Observational study of the turbulent structure of the atmospheric boundary layer under stable conditions, J. Meteorol. Soc. Jpn. 57 (1979) 423–430.
[37] G. Zhu, Wind-tunnel investigation of the flow structure within a dense-gas plume, Internal Data Report, Fluid Modeling Facility, US Envir. Prot. Agency, Research Triangle Park, NC, 1995.
[38] G. Zhu, A wind tunnel investigation of the flow structure within a dense-gas plume, M.S. Thesis, Dept. of Marine, Earth and Atmospheric Sciences, North Carolina State Univ., Raleigh, NC, 1996.